Journal of Management & Entrepreneurship
ISSN 2229-5348

UGC Care Group I Journal
Vol-09 Issue-02 Nov 2020

Microwave SQUID Multiplexer Energy Pulse Readout:

Dr. Loknath Sarangi,
College of Engineering Bhubaneswar

***Abstract*—It is exceedingly difficult to find suitable procedures for reading out huge arrays of metallic magnetic calorimeters; in order to maintain the intrinsic quick signal rise time, excellent energy resolution, large energy dynamic range, and highly linear detector response, each system stage must function at its peak. The key to accomplishing this is a superconducting quantum interference device-based multiplexer. A method known as flux-ramp modulation, which creates a phase-modulated complex waveform based on the sensor data, is necessary for the response to be linear. Currently, it is retrieved at the conclusion of the signal processing chain by a demodulation method known as Fourier measurement. This letter presents an alternative approach based on the eigenvalue decomposition of a correlation matrix, establishes the equivalenty between the mentioned method and a maximum likelihood estimation, builds an analogy to the sensor array-based direction of arrival estimation, presents the mathematical formulation, discusses the results, and compares the two approaches. Our technique enables accurate estimation across a wide phase range and is resistant to transients caused by the flux ramp returning point.**

***Index Terms*—Array signal processing, eigenvalue decomposition, microwave SQUID multiplexer, neutrino mass investigation.**

I. Introduction

MICROWAVE SQUID multiplexing (μMUXing) is currently a research topic of the highest importance since it allows the readout of large low-temperature sensor arrays [1], [2]. In recent years, a great effort has been made to demonstrate the feasibility of small array multiplexer systems which can scale up to hundreds/thousands of pixels like, for instance, metallic magnetic calorimeters (MMC) [3]–[5].

MMCs are cryogenic detectors operated at temperatures well bellow 100 m K, typically 10 m K $\leq T \leq$ 30 m K. They are composed of a particle absorber with heat capacity C strongly coupled to a temperature sensor which has a weak thermal link G to a thermal bath [6], [7]. MMCs use a metallic, paramagnetic temperature sensor located in a weak magnetic field to convert the temperature deviation ΔT into magnetic flux variation $\Delta\Phi$. The change on the detector temperature due to an energy input leads to a change of the sensor magnetization, and consequently, intensify or mitigate the magnetic flux threading a pickup coil [6], [7]. This detectors deserve special attention for their excellent energy resolution, fast intrinsic signal rise time (values below 100 ns), large energy dynamic range as well as highly linear detector response [5]. These are characteristics that underlie its usage on several knowledge fields including high-resolution X-ray spectroscopy in atomic and nuclear physics [8], [9], radiation metrology [10], direct Neutrino mass investigation [11], [12], among others.

The magnetic flux variation is sensed by a superconducting quantum interference device (SQUID). In principle, a single non-hysteretic SQUID acts like a magnetic flux controlled variable inductance $L(\Phi)$, so that it is inductively coupled to the termination of a quarter-mode superconducting transmission line with nominal resonant frequency f_r in the GHz range. As a consequence of the resonator capacitive coupling to a feed line and the inductive termination, the branch will have an effective resonant frequency f_e [13]. Optimization of physical resources is achieved by attaching two pixels to a single SQUID, providing positive or negative pulses.

The μMUXing strategy consists of reusing the mentioned structure based on a frequency division multiplexing (FDM) technique. The multiplexer and the processing system communicate by a read out electronics developed specifically for this purpose. The Electron Capture in ^{163}Ho experiment (ECHo) is a great example of such system implementation. Several non-hysteretic, unshunted rf-SQUIDs modulate the detector signals onto carriers ranging from 4G Hz to 8GHz, see [12]. A software-defined radio (SDR) was completely developed to tackle the system requirements as described in [14], [15].

A technique to linearize the SQUID response is mandatory, a flux-ramp modulation is applied to all SQUIDs, which can be sinusoidal-, sawtooth- or triangle-shaped [2], [14], [16]. It continuously modulates a complex carrier in magnitude and phase by shifting f_e forwards and backwards, in addition, energy inputs from energetic particles contribute on the actual flux state of the respective SQUID. Therefore, each μMUXing channel is a single-input single-output (SISO) system, and the pulse information could be retrieved from the data set. Fig. 1 shows the complete system including the SDR strategy.

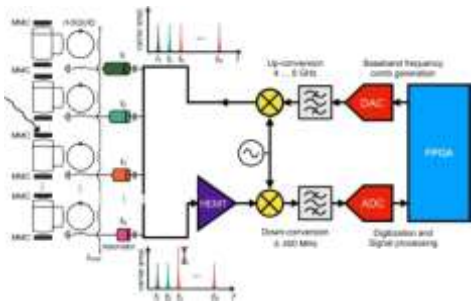

Fig. 1. Schematic representation of the SDR strategy, the μMUXing, and carrier flow.

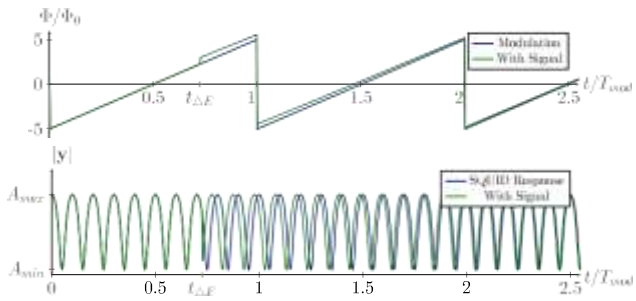

Fig. 2. Top: sawtooth-shaped ramp without (blue) and with event (green). Bottom: typical SQUID response's magnitude to the applied flux (blue) and in case an event occurred (green). The pulse duration is significantly reduced for the sake of clarity. It is usually between 10 and 100 flux ramp cycles.

We then assume that the system consists of N transmission lines and there are two MMCs coupled to each SQUID. For simultaneous readout of $2N$ pixels, there are N resonant circuits. Each circuit will be associated biunivocally to a carrier tuned to a specific frequency, so that a frequency comb is fed into a common feedline. The frequency comb is generated in a field-programmable gate array (FPGA) and mixed to a local oscillator (LO) at the radio frequency (RF) front-end, it is adjusted to slightly mismatch the resonators' frequencies. After each carrier is modulated by the respective SQUID response, it follows the path to a high electron mobility transistor (HEMT) amplifier [5]. Finally, the carriers are down-converted using the same LO frequency and the channelization is performed by the FPGA. The pulse information is available on the phase-modulated SQUID response, either to process it online or for saving the data in a storage device [15].

Great results have being achieved so far, however, extracting the pulse signal from the SQUID response can be challenging and should be carefully handled in order to preserve the signal's bandwidth. In this way, the flux-ramp modulation has posed new problems and few authors have addressed the signal processing at this step of the system chain.

In this letter, we discuss the phase estimation method presented in [16], we also propose an alternative approach based on the eigenvalue decomposition (EVD) and compare their performances. Our method arises from the analogy with the sensor array-based direction of arrival (DOA) estimation, since both of them deal with phase/frequency estimation.

This work is organized as follows: Section II focuses on the flux-ramp modulation and the respective SQUID response, as well as its demodulation process. Section III describes our proposal based on the EVD of a correlation matrix applied to the phase-shift estimation. Section IV present the main results for measured and simulated data. Finally, Section V draws the conclusion and brings suggestions for future work.

II. Theoretical Framework - Flux-Ramp (De)Modulation

The flux-ramp modulation strategy was successfully introduced to read out multiple SQUID responses on the context of an FDM technique [16]. The ramp is not infinite, thus, we consider a sawtooth or a triangular wave with period T, an observation window $T_0 < T$, and discard the samples affected by ramp-reset transient [16].

Assuming the slope of the ramp exceeds the slew rate of any input signal, the phase of the SQUID response is:

$$\varphi = 2\pi \frac{\Phi_{in}}{\Phi_0}, \tag{1}$$

where $\Phi_0 = 2.067fWb$ is the magnetic flux quantum.

In (1) the instantaneous phase is a function of the input signal and the SQUID response will be periodic with cycles determined by Φ_0. In Fig. 2 we present a sawtooth ramp and the periodic SQUID response.

In [16] the authors refer to a simple Fourier measurement which is used to estimate the phase shift of the SQUID response's magnitude, however, this is an imprecise denomination. We now deliver the maximum likelihood (ML) method applied to flux-ramp demodulation, with mathematical thoroughness, and prove that both are the same.

If the resulting waveform due to (1) could be modeled as an essentially sinusoidal wave, then we assume the phase shift is unknown and deterministic and proceed as follows [17].

In general terms, a received carrier $r(t)$ is represented by its orthonormal expansion $\mathbf{r}$, and given the reference carrier $s(t;\boldsymbol{\theta})$ with delay τ and phase φ in $\boldsymbol{\theta} = \{\tau, \varphi\}$ the probability density function is written as [17]:

$$p(\mathbf{r}|\boldsymbol{\theta}) = \left(\frac{1}{2\pi\sigma}\right)^{N} \exp\left[-\sum_{n=1}^{N} \frac{[r_n - s_n(\boldsymbol{\theta})]^2}{2\sigma^2}\right], \tag{2}$$

where $r_n = \int_T r(t)\psi_n(t)\mathrm{d}t$, and $s_n(\boldsymbol{\theta}) = \int_T s(t;\boldsymbol{\theta})\psi_n(t)\mathrm{d}t$, are the coordinates of vectors $\mathbf{r}$ and $\mathbf{s}$ from the orthonormal expansions of $r(t)$ and $s(t;\boldsymbol{\theta})$ within T_0 (integration range). The noise $e(t)$ is considered to be zero-mean white Gaussian.

Making $N \to \infty$, the maximization of $p(\mathbf{r}|\boldsymbol{\theta})$ with respect to the carrier phase φ, considering null delay ($\tau = 0$), is equivalent to maximizing the likelihood function:

$$\Lambda(\varphi) = \exp\left[-\frac{1}{N_0}\int [r(t) - s(t;\varphi)]^2 \,\mathrm{d}t\right]. \tag{3}$$

The cross-correlation alone is of interest, and the likelihood function can be written as:

$$\Lambda(\varphi) = C \exp\left[\frac{2}{N_0}\int_{T_0} r(t)s(t;\varphi)\,\mathrm{d}t\right], \tag{4}$$

where C is constant and independent of φ.

The ML estimate $\hat{\varphi}_{ML}$ is the value φ that maximizes (4), or equivalently, is the value that maximizes the logarithm of $\Lambda(\varphi)$, known as the log-likelihood function [17]:

$$\Lambda_L(\varphi) = \frac{2}{N_0} \int r(t)s(t;\varphi)\, dt. \quad (5)$$

Now, restricting the analysis to the flux-ramp demodulation, as long as the SQUID response frequency f_{SR} is known, the waveform can be represented as:

$$r(t) = A\cos(2\pi f_{SR}t + \varphi) + e(t). \quad (6)$$

The sought parameter is the value φ that maximizes (5), so that the derivative must be zero, which yields the expression:

$$\int r(t)\sin(2\pi f_{SR}t + \hat{\varphi}_{ML})\, dt = 0. \quad (7)$$

Finally, using the arc sum of a sine function, and defining a sampled version of the phase-modulated SQUID response as $\mathbf{y}_M(n) \equiv \mathbf{r}(n) = A\cos(2\pi f_{SR}T_S n + \varphi) + \mathbf{e}_M(n)$, where T_S is the sampling period, the phase parameter is given by [17]:

$$\hat{\varphi}_{ML}(n) = -\arctan\frac{\sum_{n=1}^{N}\mathbf{y}_M(n)\sin(2\pi f_{SR}T_S n)}{\sum_{n=1}^{N}\mathbf{y}_M(n)\cos(2\pi f_{SR}T_S n)}. \quad (8)$$

III. Sensor Array-Based Signal Processing

Our proposal is an analogy to the DOA problem, where several sensors record signal samples in space domain [18]. Consider in μMUXing that each resonator is a subsystem, there will be only one source $M = 1$ (the SQUID/pixels compound), and one communication channel $K = 1$ (the carrier bandwidth). To apply the DOA theory to the μMUXing estimation problem, we set a virtual sensor as a reference. This reference is obtained from the SQUID response for an idle system, i.e., no temperature change, no phase shift. Let the row vector $\mathbf{x}_R(n)$ be the reference for the non-modulated complex SQUID response and $\mathbf{x}_M(n)$ the phase-modulated response. Considering that the waveforms are harmed by a zero-mean white Gaussian noise, the reference and modulated SQUID responses are expressed respectively as:

$$\mathbf{y}_R(n) = \mathbf{x}_R(n) + \mathbf{e}_R(n); \quad (9)$$

$$\mathbf{y}_M(n) = \mathbf{x}_M(n) + \mathbf{e}_M(n). \quad (10)$$

The data matrix $\mathbf{Y}_{2\times N}$ (snapshot matrix in DOA), is set by concatenating the time series relative to each sensor as follows:

$$\mathbf{Y}(n) = \begin{matrix}\mathbf{y_R}(\mathbf{n}) \\ \mathbf{y}_M(n)\end{matrix}_{2\times N}, \quad (11)$$

so that the spatial correlation matrix $\mathbf{R}_{2\times 2}$ is estimated by:

$$\mathbf{R}(n) = \frac{1}{N}(\mathbf{Y}(n)\,\mathbf{Y}^*(n)) = \begin{matrix}\frac{\langle \mathbf{x}_R(n), \mathbf{x}_R(n)\rangle}{N} + \sigma_e^2 & \frac{\langle \mathbf{x}_M(n), \mathbf{x}_R(n)\rangle}{N} \\ \frac{\langle \mathbf{x}_R(n), \mathbf{x}_M(n)\rangle}{N} & \frac{\langle \mathbf{x}_M(n), \mathbf{x}_M(n)\rangle}{N} + \sigma_e^2\end{matrix}, \quad (12)$$

where $\langle \bullet, \bullet \rangle$ is the complex inner product, $(\bullet)^*$ denotes the conjugate transposition and N is the number of samples. The (n) indicates the sampling instant of the first entry in a data vector. Henceforth, it will be omitted for the sake of simplicity.

The spatial correlation matrix depends on the auto-correlations of $\mathbf{x}_R$ and $\mathbf{x}_M$ and the cross-correlation between them. Therefore, $\mathbf{R}$ can be written as:

$$\mathbf{R} = \frac{1}{N}\begin{matrix}|\mathbf{x}_R|^2 + N\sigma_e^2 & \langle \mathbf{x}_R, \mathbf{x}_M\rangle^* \\ \langle \mathbf{x}_R, \mathbf{x}_M\rangle & |\mathbf{x}_M|^2 + N\sigma_e^2\end{matrix}, \quad (13)$$

The characteristic polynomial provides the eigenvalues in terms of the mean power and the cross-correlation between $\mathbf{x}_R$ and $\mathbf{x}_M$. After performing some simplifications and discarding negligible terms, the eigenvalues are given by:

$$\lambda_1 \approx \frac{1}{2N}\left(|\mathbf{x}_R|^2 + |\mathbf{x}_M|^2 + 2|\langle \mathbf{x}_R, \mathbf{x}_M\rangle|\right) + \sigma_e^2, \quad (14)$$

$$\lambda_2 \approx \frac{1}{2N}\left(|\mathbf{x}_R|^2 + |\mathbf{x}_M|^2 - 2|\langle \mathbf{x}_R, \mathbf{x}_M\rangle|\right) + \sigma_e^2. \quad (15)$$

Thus, at least theoretically, the difference between both eigenvalues is immune to the noise effects, similarly to what happens in SEAD method on DOA [19]. However, experiments have shown that λ_1 fails to provide the phase estimates. We therefore assume λ_2 as a phase-shift estimator [20].

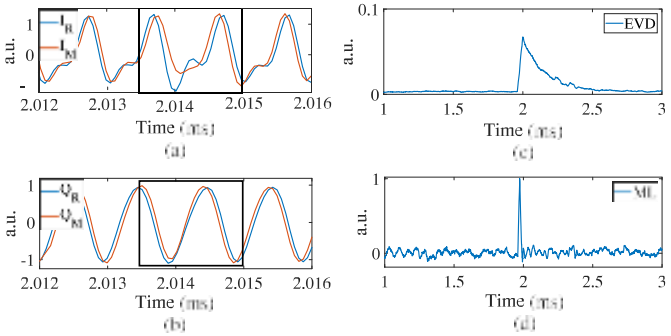

Fig. 3. Considering a triangular ramp, left side shows the (a) I and (b) Q components from the measured SQUID response, and right side presents the respective (c) EVD and (d) ML estimates. The phase shift relative to the rising ramp slope has opposite signal compared to the descending ramp slope.

IV. Experimental Setup, Evaluation and Results

In this section, we report on the estimation results from simulations performed in Matlab and from measured data. The experimental setup is the same presented in [14]. After channelization, the SQUID response has in-phase and quadrature (*I/Q*) components and both are phase-modulated. In Fig. 3 we present some results from measured data. The measurement setup had a sampling frequency $f_S = 15.625$ MHz after channelization, the flux was a triangle-shaped ramp with frequency $f_{ramp} = 25$ kHz, and peak amplitude $A_{ramp} = 6\Phi_0$, furthermore, a data block is of length $f_S/f_{ramp} = N = 625$. On the left side of Fig. 3, we present the *I/Q* components of the SQUID response with normalized magnitude ($\|\mathbf{y}\| = 1$), and, on the right side, the estimated pulse from both assessed methods applied to the measured data. The rise time of the estimated pulse, whether using the ML or the EVD, depends directly on the data amount N, i.e., one flux ramp cycle $\tau_{rise} = 40\ \mu$s. EVD allows the estimation without special procedure for both sawtooth and triangular ramps. However, this does not hold for the ML method, because the flux ramp introduces transients near to its reset point and the carrier undergoes an unexpected behavior [16]. Specially for the triangle ramp, during the pulse activity, the phase gets abruptly delayed or advanced according to the flux

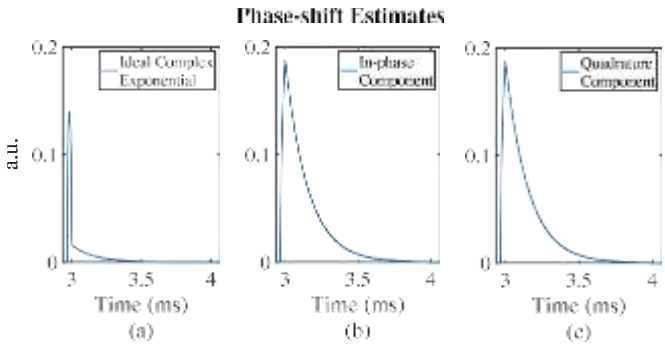

Fig. 4. Estimates using EVD for (a) complex SQUID response or its (b) in-phase and (c) quadrature components.

ramp slope, as highlighted in Fig. 3. Therefore, ML demands additional resources in order to estimate the phase shift, on the contrary, EVD method performs the estimation without further processing.

In Fig. 4, we modeled the SQUID response as an ideal complex exponential in the absence of noise. Simulations were performed considering a sampling frequency f_S = 15.625 MHz, a sawtooth modulation with frequency f_{ramp} = 25 kHz, and peak amplitude A_{ramp} = 5Φ_0, an arbitrarily chosen phase shift $\varphi = 24^\circ$, and a block length $f_s/f_{ramp} = N = 625$. The eigenvalue method is able to estimate the phase shift from both real and complex responses. All three estimates presented a long rise time (τ_{rise} = 40 μs) proportional to the number of points used in the data vector.

In order to assess the performance of the methods, we simulated them for multiple SNRs and amplitudes of phase shift, which represents different energy inputs. After scaling the maximum amplitudes of the pulses to one, we computed the mean square error (MSE) between the original and estimated pulses over the decay time interval. We performed 20 experiments for each of the different scenarios shown in the error surfaces in Fig. 5. Low MSEs indicate suitable estimates.

Fig. 5(a) shows that, when the SQUID response is modeled as ideal complex exponentials, the EVD produces suitable pulses in a long phase shift range (-1000°, 1000°). It also shows that the smaller the phase shift, the greater the influence of noise. Furthermore, for very large phase shifts the pulse shape gets distorted and larger errors are observed. Thus, there is an optimal region for pulse estimation using the proposed method. This holds for both negative and positive pulses. On the other hand, the ML method fails to estimate in this case, since the SQUID response's magnitude fluctuates around 1.

Actually, after channelization, the SQUID response components are not pure sinusoidal waves, so the dominant frequencies in I and Q may differ from each other. To the best of our knowledge, an important case arises when the frequencies differs by a factor of 2. Fig. 5(b) and 5(c) show the performances for both methods setting the in-phase frequency f_i = 300 kHz and the quadrature frequency f_q = 600 kHz. In this case, Fig. 5(b) shows that EVD estimates were effective for phase-shift magnitudes in the range (-100°, 100°) and SNRs above 5dB. EVD had a minimum MSE lower than that of the ML method. It also

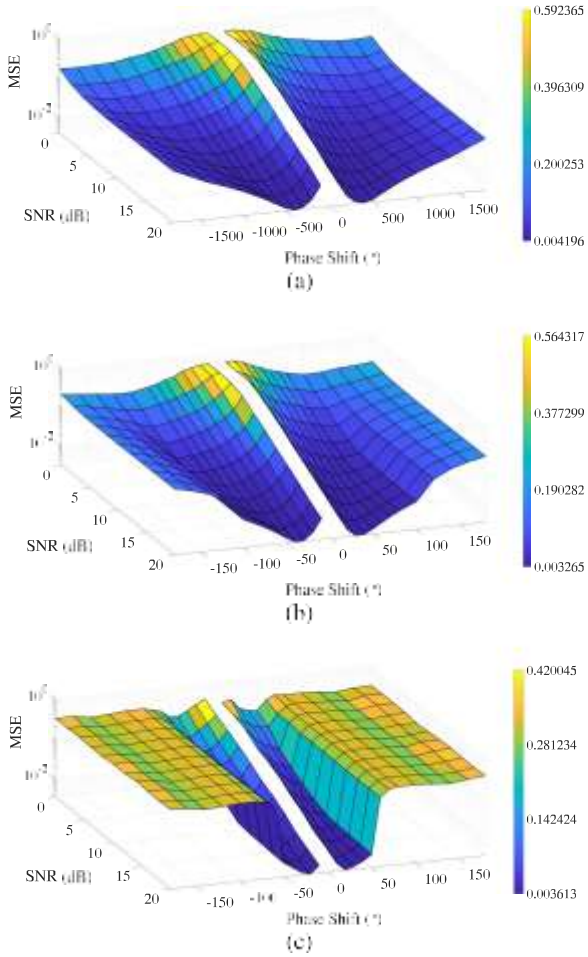

Fig. 5. Performance surfaces for (a) EVD over ideal complex exponential SQUID response, (b) EVD over a complex SQUID response with different frequencies, and (c) ML over the SQUID response's magnitude with different frequencies [20].

provided better estimates than in the case where the SQUID response was modeled as ideal complex exponentials. Fig. 5(c) shows that the ML has shown good robustness against noise and performed well in the range (-50°, 50°). However, due to the arc-tangent function range limitation, the pulse gets distorted and the ML estimation fails outside (-90°, 90°).

V. Conclusions and Remarks

This letter demonstrated for the first time that the mentioned Fourier measurement method is, in fact, the maximum likelihood estimator, using a thorough mathematical analysis of phase-shift estimation due to flux-ramp modulation. Furthermore, we utilized a sensor array technique to demonstrate that the correlation matrix's second eigenvalue is a competitive phase-shift estimator that significantly influences μMUXing, as it exhibits resilience against ramp transients and a wider energy dynamic range. Although more research is necessary, this strategy is a strong contender to address the multiple SQUID per regulator architecture and create a multiple-input multiple-output (MIMO) system, as the analogy to DOA estimation indicates.

REFERENCES

[1] K. D. Irwin and K. W. Lehnert, "Microwave SQUID multiplexer," *Appl. Phys. Lett.*, vol. 85, no. 11, pp. 2107–2109, Sep. 2004.

[2] J. A. B. Mates *et al.*, "Demonstration of a multiplexer of dissipationless superconducting quantum interference devices," *Appl. Phys. Lett.*, vol. 92, no. 2, pp. 1–3, Jan. 2008.

[3] S. Kempf *et al.*, "Design, fabrication and characterization of a 64 pixel metallic magnetic calorimeter array with integrated, on-chip microwave SQUID multiplexer," *Supercond. Sci. Technol.*, vol. 30, no. 6, pp. 1–16, May 2017.

[4] S. Kempf *et al.*, "Demonstration of a scalable frequency-domain readout of metallic magnetic calorimeters by means of a microwave SQUID multiplexer," *AIP Adv.*, vol. 7, no. 1, pp. 1–8, Jan. 2017.

[5] M. Wegner *et al.*, "Microwave SQUID multiplexing of metallic magnetic calorimeters: Status of multiplexer performance and room-temperature readout electronics development," *J. Low Temp. Phys.*, vol. 193, pp. 462–475, Feb. 2018.

[6] S. Kempf *et al.*, "Physics and applications of metallic magnetic calorimeters," *J. Low Temp. Phys.*, vol. 193, pp. 365–379, Mar. 2018.

[7] S. Kempf *et al.*, "Multiplexed readout of MMC detector arrays using non-hysteretic RF-SQUIDs," *J. Low Temp. Phys.*, vol. 176, pp. 426–434, Aug. 2014.

[8] D. Hengstler *et al.*, "Towards FAIR: First measurements of metallic magnetic calorimeters for high-resolution X-ray spectroscopy at GSI," *Phys. Scr.*, vol. 2015, no. T166, Nov. 2015, Art. no. 014054.

[9] A. Fleischmann *et al.*, "Metallic magnetic calorimeters (MMC): Detectors for high-resolution X-ray spectroscopy," *Nucl. Instrum. Method Phys. Res.*, vol. 520, no. 1, pp. 27–31, Mar. 2004.

[10] M. Loidl *et al.*, "Metallic magnetic calorimeters for absolute activity measurement," *J. Low Temp. Phys.*, vol. 151, no. 1, pp. 1055–1060, Jan. 2008.

[11] L. Gastaldo *et al.*, "The electron capture in ^{163}Ho experiment ECHo," *J. Low Temp. Phys.*, vol. 176, pp. 876–884, May 2014.

[12] L. Gastaldo *et al.*, "The electron capture in ^{163}Ho experiment - ECHo," *Eur. Phys. J. Special Topics*, vol. 226, pp. 1623–1694, Jun. 2017.

[13] J. A. B. Mates, "The microwave SQUID multiplexer," Ph.D. dissertation, Dept. Physics, Univ. Colorado, Boulder, CO, USA, 2011, p. 128.

[14] O. Sander *et al.*, "Software-defined radio readout system for the ECHo experiment," *IEEE Trans. Nucl. Sci.*, vol. 66, no. 7, pp. 1204–1209, Jul. 2019.

[15] N. Karcher *et al.*, "SDR-based readout electronics for the ECHo experiment," *J. Low Temp. Phys.*, vol. 200, pp. 261–268, Apr. 2020.

[16] J. A. B. Mates *et al.*, "Flux-ramp modulation for SQUID multiplexing," *J. Low Temp. Phys.*, vol. 167, pp. 707–712, Feb. 2012.

[17] J. G. Proakis and M. Salehi, "Carrier and symbol synchronization," in *Digital Communications*, 5th ed., New York, NY, USA: McGraw-Hill, 2008, ch. 5, sec. 1/2, pp. 290–315.

[18] R. P. Lemos *et al.*, "Using matrix norms to estimate the direction of arrival of planar waves on an ULA," *J. Franklin Inst.*, vol. 356, no. 9, pp. 4949–4969, Jun. 2019.

[19] H. V. L. Silva *et al.*, "A branch-and-bound inspired technique to improve the computational efficiency of DOA estimation," *Signal Process.*, vol. 93, no. 4, pp. 947–956, Apr. 2013.

[20] J. A. Kunzler, "Development and analysis of mathematical methods for estimating statistical parameters in sensor array-based systems," Ph.D. dissertation, Dept. Elect., Mech., Comput. Eng., Fed. Univ. Goias, Goiania, GO, Brazil, 2020.